ACS Photonics

pubs.acs.org/journal/apchd5

Article

Photonic Crystal Waveguides for >90% Light Trapping Efficiency in Luminescent Solar Concentrators

Haley C. Bauser,[†] Colton R. Bukowsky,[†] Megan Phelan, William Weigand, David R. Needell, Zachary C. Holman, and Harry A. Atwater*

Cite This: https://dx.doi.org/10.1021/acsphotonics.0c00593

Read Online

ACCESS | Metrics & More | Article Recommendations

ABSTRACT: Luminescent solar concentrators are currently limited in their potential concentration factor and solar conversion efficiency by the inherent escape cone losses present in conventional planar dielectric waveguides. We demonstrate that photonic crystal slab waveguides tailored for luminescent solar concentrator applications can exhibit >90% light trapping efficiency. This is achieved by use of quantum dot luminophores embedded within the waveguide that absorb light at photon energies corresponding to photonic crystal leaky modes that couple to incoming sunlight. The luminophores then emit at lower photon energies into photonic crystal bound modes that enable highly efficient light trapping in slab waveguides of wavelength-scale thickness. Photonic crystal waveguides thus nearly eliminate escape cone losses, and overcome the performance limitations of previously proposed wavelength-selective dielectric multilayer filters. We describe designs for hole-array and rod-array photonic crystals comprised of hydrogenated amorphous silicon carbide using CdSe/CdS quantum dots. Our analysis suggests that photonic crystal waveguide luminescent solar concentrators using these materials these can achieve light trapping efficiency above 92% and a concentration factor as high as 100.

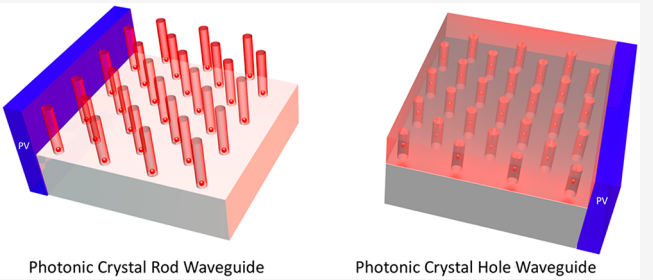

KEYWORDS: *photonic crystals, quantum dots, luminescent solar concentrators, waveguide coupling, photovoltaics*

Luminescent solar concentrators (LSCs) are of considerable interest for various solar energy conversion applications, including utility-scale photovoltaics and building integrated photovoltaics, due to their ability to effectively concentrate both direct and diffuse sunlight[1−7] and, thus, to concentrate the global solar spectrum using low cost materials.[8] LSCs consist of a waveguide medium with embedded luminophores (e.g., dyes, quantum dots, rare earth ions) that down-convert incident light and guide the down-converted light emission to a photovoltaic cell for solar energy conversion.[1−7]

Previous LSC designs suffer from low optical efficiencies, in part due to luminophores with low efficiencies and/or small Stokes shifts,[7] as well as poor waveguide trapping efficiencies. The Stokes shift, which is the difference between the luminophore absorption and emission energy,[9,10] is a key factor determining the concentration limit due to its exponential effect on the maximum achievable concentration factor.[10] The concentration factor is defined as the ratio of the optical power density that arrives at the photovoltaic cell within the LSC waveguide to the flux that arrives at the waveguide top surface.[9,10] Recent developments in LSC design, as well as high efficiency quantum dot luminophores (QDs) with large Stokes shifts, have thus opened a path to a potentially large increase in achievable LSC concentration factors.[11,12]

However, to date, the maximum achievable concentration factor has also been limited by the waveguide optics of luminescent solar concentrators. In polymer planar slab waveguides with embedded luminophores, a theoretical maximum of only 74% of the emitted light is trapped in the waveguide via total internal reflection (TIR) for a waveguide index of refraction of 1.44, which corresponds to poly(lauryl) methacrylate (PLMA) which serves as an effective dispersion medium for CdSe/CdS quantum dots.[6,11−14] The remaining 26% of emission exits the slab through the escape cone, as shown in Figure 1a. In order to overcome this source of loss, recent LSC designs have used wavelength-selective Bragg reflectors.[6,15−18] Bragg reflectors are composed of periodic stacks (typically 10s−100s of layers) with alternating refractive indices. Figure 1b shows an example of a Bragg reflector with a

Received: April 13, 2020
Published: June 19, 2020

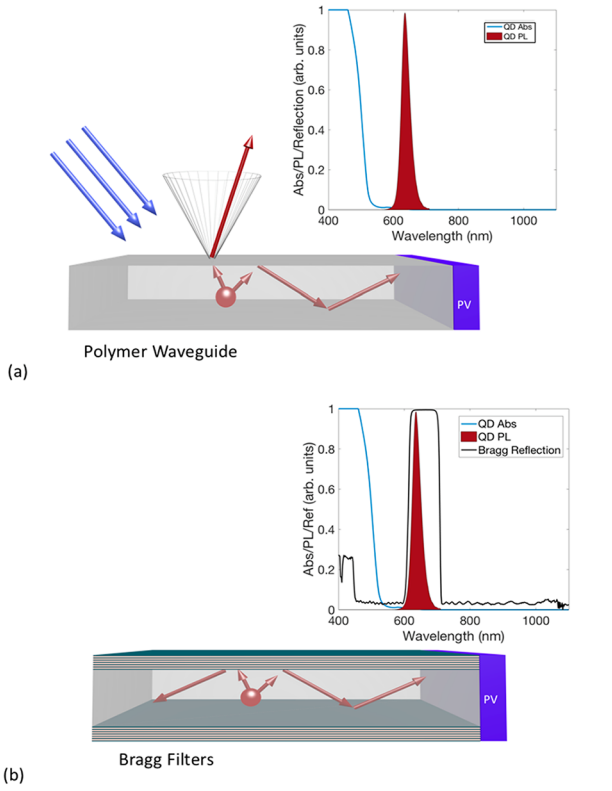

Figure 1. QD emission loss in several LSC configurations. In (a), isotropic QD emission is trapped only via TIR with significant escape cone losses. In (b), Bragg filters with the reflection band indicated in the inset can further trap QD emission. In (c), photonic crystal waveguide rod and hole arrays, respectively, trap emitted light in guided modes.

characteristically wide reflection band capable of trapping emission of a luminophore in a polymer waveguide at near unity efficiency.[6] However, Bragg reflectors block a portion of incident solar spectrum and exhibit significant blue shifting under increasing angles of incidence.[8,17−19] Blue shifting causes the reflection band to move to wavelengths of QD absorption, thereby limiting QD luminophore performance by blocking sunlight, which the QD would otherwise be able to convert, thus, decreasing LSC module efficiency.

In this paper, we report on photonic crystal designs to improve LSC waveguides by more efficiently trapping light in the waveguide plane. In Figure 1c,d we show photonic crystal rod and hole arrays with coupled quantum dots. As opposed to trapping light in a ray optical regime, as is shown in Figure 1a,b, we study trapping in the wave-optic regime and emission

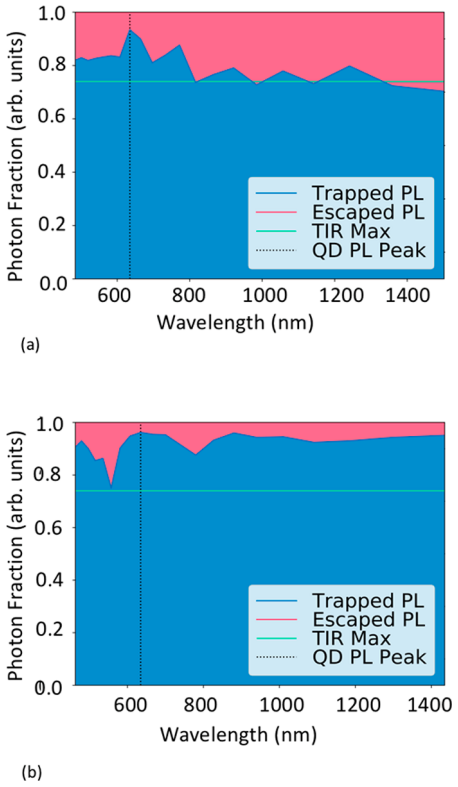

Figure 2. The left axis shows photonic crystal waveguide light trapping fraction; vertical dashed line shows the QD emission wavelength. In (a), a rod array with QDs located in the center of the pillar at the substrate interface traps over 90% of QD emission. In (b), the hole array traps over 90% of QD emission when the QD is placed in the center of the holes.

coupling into waveguide modes of photonic crystal slab structures. We report specific photonic crystal designs for both a rod array and a hole array. The arrays consist of CdSe/CdS QDs coupled to high index a-SiC:H. Figure 2 demonstrates that both rod and hole array designs are capable of trapping the CdSe/CdS QD emission at an efficiency above 90%, substantially more than the theoretical maximum of 74% achieved by TIR modes of an index 1.44 polymer. In addition to the increased trapping efficiency, this approach increases the achievable concentration factor and also has potential for decreasing the module cost by eliminating the need for wavelength selective filters. For the purpose of the paper, we will consider highly efficient CdSe/CdS QD LSC luminophores, as reported by Hanifi et al.[6,20] The absorption and luminescence emission spectra for these luminophores are recreated in Figure 3. The CdSe/CdS QDs are highly efficient with a photoluminescence quantum yield (PLQY) of 99.6% ± 0.3%, a Stokes shift of 0.52 eV, and a Stokes ratio above 100. The Stokes ratio is defined as the ratio of the absorption coefficient of the CdS shell to the absorption coefficient of the CdSe core.[20] Our LSC waveguides are thus designed to trap light emitted by the CdSe/CdS QDs.

PROPERTIES OF PHOTONIC CRYSTAL WAVEGUIDES

Guided modes in photonic crystal waveguides (PCWGs) have been extensively studied and experimentally realized for applications in magnetic mode control, nonlinear optics, high quality resonators, on-chip photonic lasers, and LSCs.[21−28]

https://dx.doi.org/10.1021/acsphotonics.0c00593
ACS Photonics XXXX, XXX, XXX−XXX

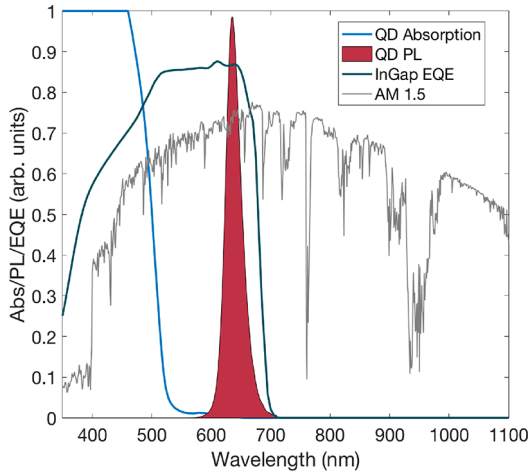

Figure 3. Absorption and photoluminescence of CdSe/CdS quantum dots. The absorption cutoff is near 500 nm and PL peak is at 635 nm. The EQE indicates the InGaP cell band edge aligns with the QD PL peak. The AM 1.5G solar spectrum is shown for reference.

PCWGs are capable of guiding emitted light into waveguide modes, thus, increasing the optical efficiency of waveguides for LSCs. For the purposes of light trapping in LSCs, we consider the 2-D PCWG that is periodic in the x and y plane with a defined thickness, t, in the z plane. PCWGs trap the transverse electric (TE) and transverse magnetic (TM) modes of luminophore light by increasing the local density of optical states (LDOS) available to an emitter.[29,30] In our design, the TM- and TE-guided modes can be tailored to have a large LDOS and achieve the highest possible chance of light remaining trapped in the PCWG. We therefore analyze both hole and rod waveguides in parallel.

In our evaluation of PCWG perfomance, we also consider Purcell enhancement and the resulting Purcell factor, F_p, generated in the photonic slab waveguide. The Purcell factor, given in eq 1, refers to the proportional increase in the spontaneous rate or emission of a dipole, as a function of the environment in which the emitter is placed, where V is the mode volume within the crystal and λ_{free}/n is the wavelength within the PCWG.

$$F_p = \frac{3}{4\pi^2}\left(\frac{\lambda_{free}}{n}\right)^3\left(\frac{Q}{V}\right) \quad (1)$$

Q is the quality factor that we more specifically define in eq 2, where f_0 is the frequency within the photonic crystal (PC), E is the energy within the PC, and P is the dissipated power within the PCWG.

$$Q = \frac{2\pi f_0 E}{P} \quad (2)$$

This result follows from Fermi's Golden Rule and predicts that placing a QD emitter in a nanostructured dielectric environment with a large LDOS enhances spontaneous emission into specific optical modes relative to emission into free space.[30−36] Our simulation results use eq 1 and the simulated dipole power emitted at various positions of a PC to determine F_p. Within the utilized Lumerical software, the Purcell factor calculation is simplified to be the ratio of the dipole within the PCWG to the dipole power in free space.[32−35]Due to detailed balance between photon absorption and emission, the converse is also true: emission into lossy modes and/or excited carrier thermalization losses can be reduced.[31,36−38]

$$\mathrm{PLQY}_{enhanced} = \frac{F_p \times \mathrm{PLQY}_0}{F_p \times \mathrm{PLQY}_0 + (1 - \mathrm{PLQY}_0)} \quad (3)$$

Nonradiative losses are thus reduced, increasing the PLQY of the QDs, as indicated in eq 3. By placing the QD in a photonic crystal with a modest Purcell factor (3−5), highly efficient QDs (PLQY > 90%), such as the CdSe/CdS dots, can exhibit a PLQY closer to unity.[39] Likewise, if we can achieve higher Purcell factors (>8), less efficient QDs (PLQY < 70%) can increase their PLQY to above 90%, illustrated in Figure 4.

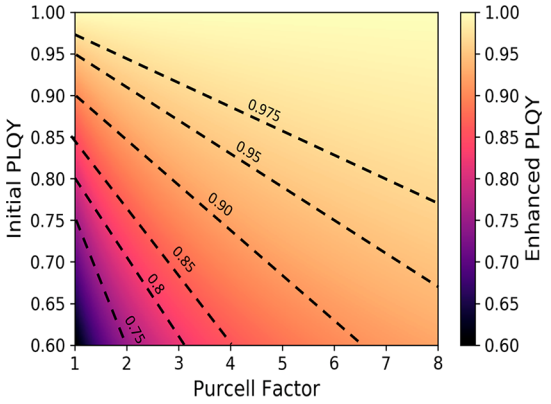

Figure 4. Enhancement of QD PLQY as a function of Purcell factor.

The phenomenon of Purcell enhancement via PCWGs holds great potential for the LSC community as many QDs that absorb a greater portion of the solar spectrum and emit at longer wavelengths suffer from decreased PLQYs.[11,40,41] The Purcell enhancement provided by a PCWG can thus be applied to systems with near-infrared emitting QDs tuned to photovoltaic material such as GaAs or Si, which could in turn increase the overall device efficiency.[42] The design parameters of the PCWG can be rescaled in order to accommodate different emission wavelengths. We therefore analyze both the trapping potential and the Purcell enhancement of photonic crystals with coupled QDs.

PHOTONIC CRYSTAL DESIGN

In order to design an experimentally realizable LSC system, the photonic crystal design should consider realistic materials properties and fabrication limitations related to the slab thickness and QD location within the waveguide. It has previously been shown that a z mirror symmetric 2D photonic crystal slab in air maximizes mode confinement and, in turn, achieves minimal light leakage.[29,30] Here we must include a substrate on which the photonic crystal material can be deposited. By including a substrate layer, the z symmetry of the photonic crystal is broken, introducing newly accessible leaky modes to the photonic crystal as TE and TM modes couple to each other and are no longer trapped within the photonic crystal plane.[29] Instead, light can escape the photonic leaky modes and couple into waveguide modes of the underlying $n > 1$ index substrate.[29,30] This provides a mechanism for collection within the LSC system of the light leaking to the substrate. Thus, our design creates a preference for emission into PC slab guided modes and the TIR guided modes of the substrate. Since light emitted outside the angle of the substrate

https://dx.doi.org/10.1021/acsphotonics.0c00593
ACS Photonics XXXX, XXX, XXX−XXX

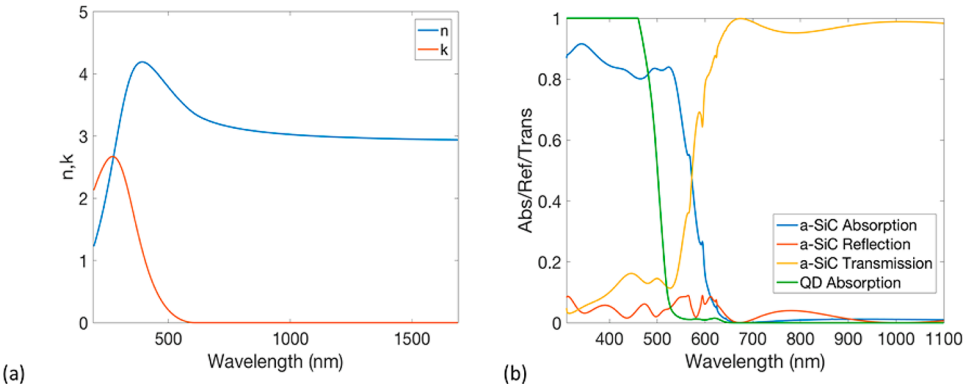

Figure 5. In (a), index of refraction and extinction coefficient of a-SiC:H, measured via spectroscopic ellipsometry. In (b), reflection, absorption, and transmission of a hexagonal array PCWG of a-SiC:H pillars at a sufficient trapping thickness. QD absorption is also shown to indicate an overlap in absorption of the QDs and the photonic crystal material.

escape cone stays trapped within the substrate TIR modes, we consider that light to also be trapped, in addition to light that is trapped within the plane of the photonic crystal material. There are multiple photovoltaic cell configurations that can utilize the light trapped in both the photonic crystal and the substrate plane, so light traveling laterally in either layer effectively stays within the LSC system. Thus, the total trapping efficiency is the percentage of emitted light trapped either in the PCWG or the substrate, whereas photons lost to the ambient environment are considered lost from our PCWG system.

The second parameter we consider is the absorption wavelengths of the QDs in relation to that of the photonic crystal material. In order to achieve a high Purcell enhancement, it is advantageous for the photonic crystal to be created from a high index material which also has low absorption, so as to avoid parasitic absorption of light emitted from the QDs into the photonic crystal slab.[31−37] Our high index PCWGs are based on plasma enhanced chemical vapor deposited a-SiC:H that has negligible absorption beyond 610 nm, while maintaining an index of refraction greater than 3 across the PL spectrum.[43] The disadvantage to using this material is its high absorption in the short wavelength region; as previously described, CdSe/CdS QDs absorb light with wavelengths up to 500 nm. The slab material and the QDs both absorb short wavelength light, as shown in Figure 5. Previous work has explored directly embedding luminophores in visibly transparent, lower index materials, like TiO_2 or ZnS; however, the low index leads to lower trapping efficiencies and lower Purcell enhancement.[39] Furthermore, even though the absorption length is decreased for the lower index materials, there is still some absorption, so less light is absorbed and converted by the QDs, which in turn results in a less-efficient module. Therefore, we choose to work with the higher index a-SiC:H, but change the QD placement accordingly in the rod array to mitigate parasitic absorption. We cannot locate QDs inside the pillars of the rod array. In order to ensure as much light as possible reaches the QDs to be successfully down-converted, we thus opt to locate the QD layer at the bottom of the photonic crystal rod array slab waveguide at the substrate interface. With the QDs at the substrate interface, the rod array orientation is inverted, with the substrate becoming a superstrate. With this inversion, incoming light will first travel through the superstrate before reaching the QDs, as opposed to traveling through the a-SiC:H. This will allow the vast majority of incoming short wavelength light to be absorbed and re-emitted by the QDs before having the chance to be parasitically absorbed by the a-SiC:H. Once the QD re-emits, the emission will travel via the PCWG, which is lossless in the emission region, and the TIR modes of the substrate. We thus opt for this inverted configuration, in contrast with placing the QDs at the top of the pillars at the air interface, in order to guide modes into the TIR of the glass substrate rather than emission to air. This will inevitably lead to lower trapping and Purcell enhancement than would be achievable if QDs could be located at the center of each rod, because the symmetry of the photonic crystal is broken, which furthermore decreases the mode volume and mode density within the crystal. However, this trade-off is necessary in order to build a feasible and optically efficient photovoltaic module. Such a system can potentially be fabricated by first applying a layer of dispersed QDs to the substrate and then depositing the PCWG material.[44−46] The use of a superstrate configuration is thus preferred to configurations in which the high energy photons are at greater risk of parasitic absorption by a-SiC:H.

In addition to the rod array, we evaluate a hole array 2D PCWG, in which the QDs are placed within holes etched into a film of a-SiC:H. The hole array 2D PCWG does not have the same QD placement constraints as for the rod array due to the QD placement outside the absorbing medium. The QDs can be located throughout the volume of the holes, as opposed to an effective single layer of QDs at a specific location, as is required for the rod array. Another advantage of the hole array is the greater effective index of refraction. Instead of setting the

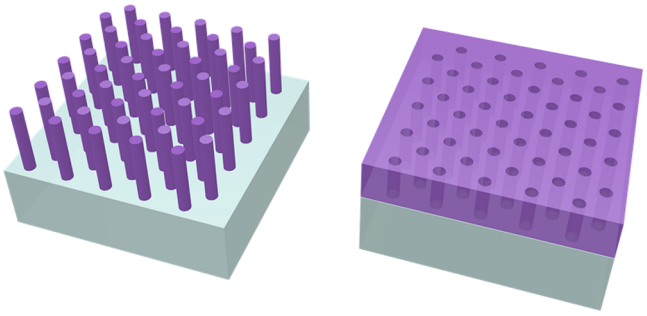

Figure 6. Schematic of the rod array (left) and hole array (right) a-SiC:H PCWGs. The rod array has a thickness of 1.21 μm, a rod radius of 61 nm, and a pitch of 242 nm. The hole array has a thickness of 694 nm, a hole radius of 58 nm, and a pitch of 231 nm.

https://dx.doi.org/10.1021/acsphotonics.0c00593
ACS Photonics XXXX, XXX, XXX−XXX

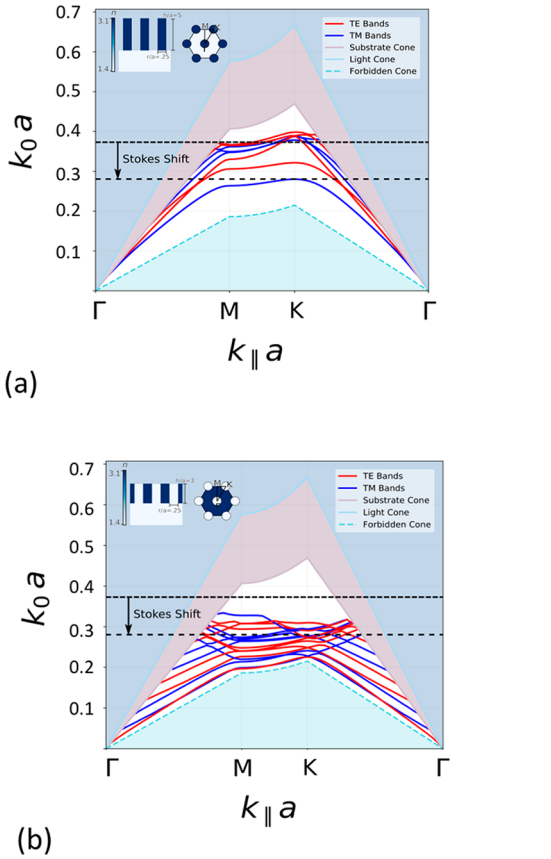

Figure 7. In (a), band structures for the optimized hexagonal rod array of a-SiC:H. The Stokes shifted QD emission couples to the TE and TM modes of the photonic crystal. In (b), band structures for the optimized hexagonal hole array PCWG composed of a-SiC:H. The Stokes shift demonstrates that the QDs emission lies within the TE and TM bands of the photonic crystal. The top right insets in both a and b show the unit cell and structure, color coded by the index of refraction of the PCWG and the surrounding material.

holes to an index of 1 to simulate air, we set it to 1.44 to simulate poly(laurel) methacrylate, a common polymer material used as a matrix for suspending CdSe/CdS QDs.[6] The higher index of refraction increases the effective index of the photonic crystal, thereby allowing for a higher potential Purcell enhancement and trapping.[31,32]

As detailed in the Methods section, the parameters for the radius, pitch, and height of both the hole array and the rod array are set in units normalized to the wavelength. For both array types, we choose a hexagonal array in order to have a higher fill fraction than a square array provides. Both the hexagonal rod array and hole array are set with radii a quarter of the periodicity.[29] We found upon exploring the hole radius parameter space that varying the hole radius did not result in drastically different trapping potentials, so therefore, kept them as a quarter of the periodicity for both arrays. While the ratios of the periodicity and radius are the same for the rod and hole array, the respective array designs deviate with respect to thickness. Since the QDs have to be placed at the substrate interface in the rod array, the photonic crystal must be thicker than the hole array in order to maximize the light trapped in the PCWG and substrate TIR modes. This corresponds to a height five times the periodicity. The hole array does not have the same thickness requirement in part due to improved trapping from the increase in waveguide effective index. The

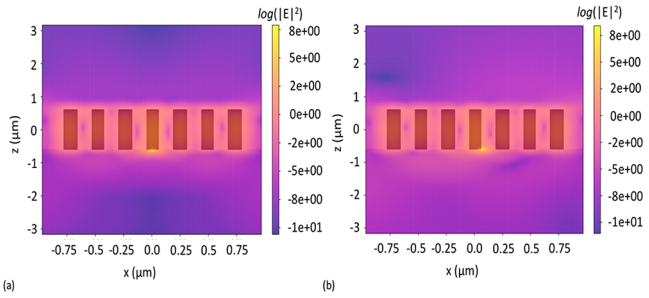

Figure 8. Magnitude of the electric field intensity of QD emission in an optimized hexagonal array of a-SiC:H rods with the QDs located at the glass interface. In order to simulate the entire area of the rod/glass interface, the QD was located in the center (a) then translated toward the edge (b) in order to optimize average trapping over the entire substrate interface containing QD emitters.

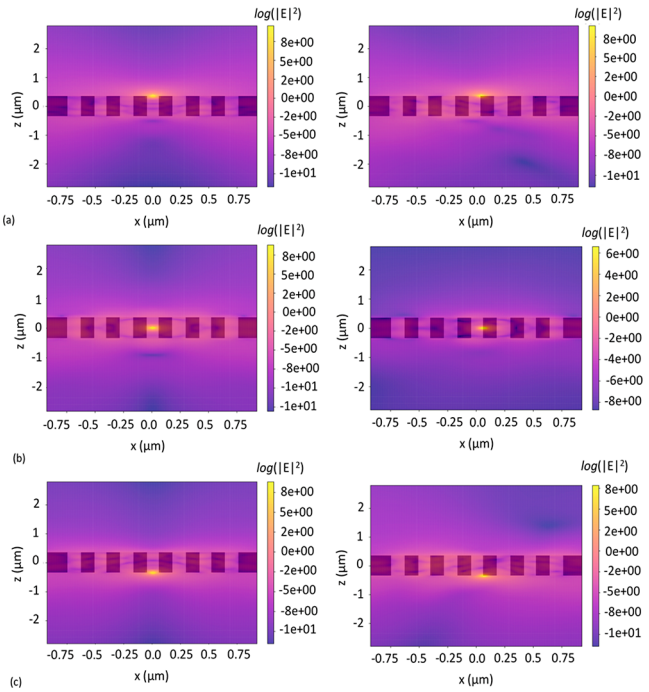

Figure 9. Magnitude of the electric field intensity for the optimized a-SiC hexagonal hole array. QD locations are translated to different x, y, and z locations to characterize QD emission trapping in the array. In (a), QD at the air interface; in (b), QD in the center of the hole array; in (c), QD emission located at the substrate interface. The left column shows the electric field intensity with the QD located in the x, y center, and the right columns shows the electric field intensity with the QD located at the edge of the hole radius for each respective z location.

trapping potential remains stable for a range of thicknesses. However, the thickness is set to three times the periodicity in order to explore a wider set of QD placements throughout the volume of the hole. To summarize, we find the optimal geometry for the rod array to be a radius of 61 nm, a pitch of 242 nm, and a height of 1.21 μm. For the hole array, we set the radius to 58 nm, the pitch to 231 nm, and the height to 694 nm, as illustrated in Figure 6. Given the index of refraction of the PCWG, the index of the substrate, and the physical designs demonstrated in Figure 6, the band diagrams in Figure 7 were generated. For both the rod and hole array, there is one or many flat TE and TM bands at the QD emission frequency.

https://dx.doi.org/10.1021/acsphotonics.0c00593
ACS Photonics XXXX, XXX, XXX−XXX

The strong coupling of luminescence to the PCWG seen in FDTD simulations is supported by the location of these bands at the PL frequency. The flat quality of the band(s) indicate a high LDOS of modes with large, in plane wave vectors, which agrees with the large percentages of light detected to travel laterally in FDTD simulations. Even though the field profiles of Figures 8 and 9 include all modes, the order and periodic quality of these photonic crystal modes is clearly recognizable.

TRAPPING EFFICIENCY

For both the rod and hole array PCWGs, we start by finding the trapping efficiency and Purcell factor for QDs located in the center for maximum symmetry. In the rod array, the highest symmetry point is the center in the x, y plane at the waveguide/substrate interface. For the hole array, the point of maximum symmetry is centered in a hole in the $x-y$ plane, and at the height midpoint within the slab. To best simulate realistic QD arrays, we locate the QDs throughout the $x-y$ symmetry plane for the rod and hole array. For the rod array, we assume the QDs will be spin-coated and therefore will cover the x, y plane of each pillar at the waveguide/substrate interface. We locate the QD at the edge of the pillar in the x and y directions, then along the arc between the x and y edges in order to get a robust data set of QD behavior through the area of the crystal/substrate interface. As shown in Figure 8, locating the QD in the center of the rod at the crystal/substrate interface results in the majority of the electric field intensity to be contained within the plane of the PCWG, with much of the light in the substrate region emitting outside the escape cone of the substrate. While locating the QD at the edge of the rod radius further breaks symmetry and does not result in as high of a trapping efficiency as the aforementioned location, the majority of the emission of the QD remains trapped within the PCWG and substrate TIR. We find that the average trapping efficiency for the rod array with QDs dispersed across the rod array area at the PCWG substrate interface is 92.56% with a Purcell factor of 2.2.

To analyze QD trapping in the hole array, we must consider the x, y, and z directions and, therefore, perform a sensitivity study over a volume of potential QD locations. Figure 9 demonstrates that the hole array maintains a similar pattern to the rod array shown in Figure 8. In all cases, the majority of the electric field intensity of the QD emission remains in the plane of the PC material with more emission loss, particularly outside the TIR modes of the substrate, introduced upon moving the QD across the x, y plane by breaking the symmetry of the PCWG. Moving the emitter position throughout the range of z values yielded interesting results, as demonstrated in Table 1. Moving the QD location toward the substrate or air interface of the photonic crystal caused the light trapping efficiency to fluctuate in proportion to the fraction of light emitted in the escape cone of the substrate. The trapping efficiency, assuming a disk-like monolayer of QDs located in the center of the a-SiC:H hole array, is 95.36%. As stated in the previous section, the total height of each pillar in the hole array is 694 nm. When moving the QD 232 nm from the center in the positive or negative direction, the trapping efficiency drops from 95.36% in the center to around 91.5% at z coordinates of 579 and 115 nm, respectively, from the substrate interface. However, when moving to 636 or 58 nm, the trapping efficiency increases to 93.82% for both heights. This results from successful trapping in either PC modes or TIR modes of the substrate. When QDS are located closer to the top or bottom of the photonic crystal, at the air or substrate interfaces, light trapping in the photonic crystal plane remains nearly constant, however the fraction of light in TIR modes of the substrate increases. Moreover, when QDs are located at a height of 115 nm above the substrate interface, approximately 85% of the emitted light stays within the photonic crystal. We observe similar behavior when we move the QD downward to 58 nm above the substrate interface. Likewise, for both QD placements, about 11% of the light travels out of the photonic crystal into the substrate. However, when the QD is located at a height 115 nm above the substrate, 44% of that light is lost via the substrate escape cone, whereas only 22% the light in the substrate is lost via the substrate escape cone for the QD placed 58 nm above the substrate.

When QDs are located near the crystal/substrate and crystal to air interface of the hole array, there is a significant reduction in light trapping efficiency. Light trapping for QDs at the air interface decreases to 82.5% and the light trapping efficiency decreases to 84.16% for QDs located at the substrate interface. Given how robust the trapping efficiency remains from 58 to 636 nm, we explored where this drop-off occurs and found that the trapping efficiency only drops below 90% within 25 nm of either interface. When accounting for a random distribution of QDs throughout the entire volume of the hole, the trapping efficiency is 92.3% with a Purcell factor of 2.9. If we assume that the polymer layer near the top and bottom interfaces is devoid of QDs, so that QDs are located only at heights from from 58 to 636 nm, the trapping efficiency increases to 93.3% with a Purcell factor of 3.2. If we lower the optical density of the QDs, allowing a lower volumetric QD concentration, we can concentrate the QDs in a thin disk located in the center of the holes with the majority of the volume infilled with polymer. This gives a trapping efficiency of 95.4% with a Purcell factor of 3.26.

Table 1. Trapping Efficiency and Purcell Enhancement as a Function of QD Location in Hole (HA) and Rod Array (RA) Photonic Crystal Waveguides

quantum dot location	η_{trap} (%)	F_p
TIR only; in waveguide	74.13	1
RA; at substrate interface	92.56	2.2
HA; in PCWG center	95.36	3.26
HA; 58 nm above substrate	93.82	3.33
HA; 638 nm above substrate	93.82	3.34
HA; 579 nm above substrate	91.80	3.24
HA; at air interface	82.50	2.64
HA; at substrate interface	84.16	2.62
HA; infill full hole volume	92.30	3.2
HA: infill 58−638 nm	93.32	3.3

While the photonic band gap is not included in our figure of merit, the difference between the TE and TM band structures in rod arrays compared to hole arrays resulted in distinctly different in trapping mechanisms. The difference in the Purcell factor is particularly notable. In the rod array, the Purcell factor of the x and y dipole emission profiles of the QD are low due in part to how the rod array favors a TM photonic bandgap. In the hole array, the x and y dipole emission profiles of the QDs exhibit higher Purcell factors, averaging over all possible dipole directions. Since the rod array favors the z-oriented dipole emissions, the trapping efficiency and Purcell factor could greatly be improved by the use of properly oriented quantum

https://dx.doi.org/10.1021/acsphotonics.0c00593
ACS Photonics XXXX, XXX, XXX−XXX

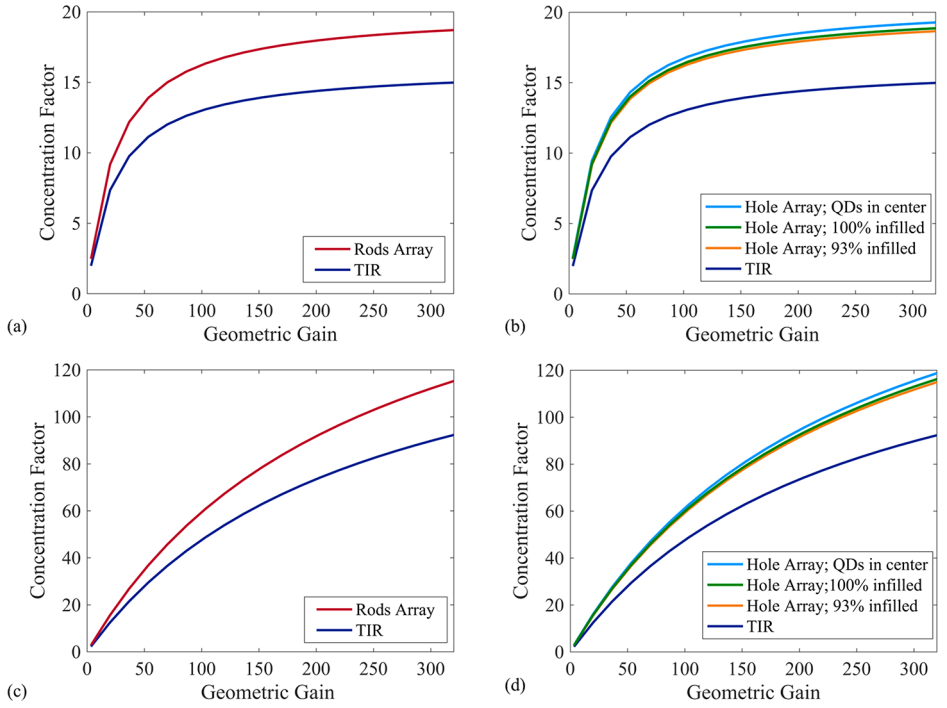

Figure 10. Concentration factor vs geometric gain for an edge-lined LSC using CdSe/CdS QDs. We show the concentration factor performance in comparison to TIR for the proposed (a) rod array and (b) hole configurations with varied ways of filling the QDs in the holes, assuming a realized Stokes ratio of 100. Figures (c) and (d) display the concentration factor performance for each the rods and holes, respectively, for an idealized CdSe/CdS quantum dot with a Stokes ratio of 1000.

rods whose emission profile more closely resembles a *z*-oriented dipole.

Both the rod array and hole array designs demonstrate that PCWGs can increase the waveguide trapping efficiency for LSCs from 74% to beyond 92%. For the rod array, we find Purcell factors of 2, while hole arrays demonstrate Purcell factors of approximately 3.

LSC CONCENTRATION FACTOR FOR PHOTONIC CRYSTAL WAVEGUIDES

We now analyze the concentration factor of LSC photonic crystal slab waveguides. Concentration factor represents the achievable enlargement factor of active PV area for an LSC.[47] LSC designs aim to achieve high concentration factors in order to minimize the required PV active area within the LSC. We define the concentration factor in eq 4 as a function of the LSC geometric gain (GG), device absorbance (η_{abs}), waveguide efficiency (η_{wg}), luminophore PLQY (η_{PL}), and trapping efficiency (η_{trap}), in accordance with an analytical analysis of concentration factor.[47] Here we define the geometric gain as the ratio of LSC area to the area of the photovoltaic cell. Analysis of the concentration factor as a function of geometric gain provides a more general figure of merit, and it is used in order to compare across different photovoltaic cell location schemes. While the highly efficient CdSe/CdS QDs display a PLQY above 99% in solution, when dispersed in a waveguide medium, the PLQY decreases to 95%.[6,12,20,48] In order to give a more experimentally relevant analysis, a PLQY of 95% is used in our concentration factor analysis. Device absorbance refers to the fraction of incident light that is absorbed by the luminophores, waveguide efficiency is the fraction of PL that reaches the PV material, and trapping efficiency is the fraction of PL trapped within waveguide modes and TIR. Hence, higher trapping efficiencies, as described in this paper, directly enable increased concentration factors.

$$\text{concentration factor} = \eta_{abs} \times \eta_{WG} \times \eta_{PL} \times \eta_{trap} \times GG \quad (4)$$

Here, we assume an LSC that uses InGaP cells with a band edge matched to the emission of the CdSe/CdS QDs,[6,9] with a measured Stokes ratio of 100,[12,20] and an optical density at 450 nm of 3.0. Here we define the Stokes ratio as the ratio of the absorption coefficient (α_1) at the QD CdS shell to the absorption coefficient (α_2) at the QD CdSe core. We analyze the concentration factor of the LSC system as a function of geometric gain. We find that increasing the trapping efficiency increases the potentially achievable concentration factors. Figure 10a shows that the concentration factor improves when employing a rod array PCWG compared to designs in which luminophores are dispersed in a polymer waveguide with only TIR light trapping. Figure 10b repeats this analysis for a hole array PCWG configuration. In Figure 10b, we compare the performance of (i) TIR alone, (ii) a disk-like array of QDs in the hole centers, (iii) filling 93% of the hole volumes with QDs, and (iv) filling the entire hole with QDs. In each of these cases, the optical density is kept constant at 3.0. We can see that higher concentration factors are achieved with the highest trapping efficiency configurations. Since the trapping efficiencies of all of these designs are >92%, each of these configurations has the potential to improve on a traditional QD waveguide by nearly 30%, which agrees with the results of Rousseau and Wood.[27]

Figure 10c and d repeat the analyses for the rod and the hole configurations, respectively, by assuming an optimized CdSe/CdS QD with a Stokes ratio of 1000. By assuming a higher Stokes ratio, we are able to achieve concentration factors

https://dx.doi.org/10.1021/acsphotonics.0c00593
ACS Photonics XXXX, XXX, XXX−XXX

beyond 100 for both the rod and the hole arrays. Furthermore, the concentration factor enhancement remains robust for the hole array infilling options, allowing for flexibility in fabrication and optical density of the QDs.

CONCLUSIONS

In this paper we have demonstrated that high index dielectric rod and hole photonic waveguides composed of a-SiC:H coupled with CdSe/CdS QDs can be used to improve the concentration factor of an LSC to more than 100. We show that over 90% of light emitted from a QD can be trapped within the modes of both a photonic crystal rod and hole slab waveguide. Employing a PCWG rod array results in a total trapping efficiency of 92.6% and a Purcell factor of 2.2. A PCWG hole array exhibits a light trapping efficiency of 95.4% for a disk-like emitter array in the hole centers for a hole array PCWG. Furthermore, we explore infilling through the z-plane of the hole array crystal and find trapping efficiencies remain above 90% for all infilling possibilities Finally, we performed a system level analysis to determine the concentration factor of an LSC is using PCWGs and found a significant increase in concentration factor as a function of geometric gain when employing nanophotonic waveguides, as compared to simply TIR mode waveguides. While high trapping and concentration factors are achieved in the proposed designs, we expect future designs and materials can be explored to further improve Purcell enhancement. A higher index polymer would also help increase the potential Purcell enhancement in the photonic crystal hole array by increasing the effective index of the photonic crystal. We further expect that, by exploring other materials and luminophores, this work can be improved upon and applied to a variety of LSC systems operating at different wavelengths that correspond to different photovoltaic materials, transmission profiles, and optical properties.

METHODS

To conduct a full analysis of both the behavior of the emitted light and the module performance, we use two different analysis methods. First, we employ Lumerical FDTD simulations to calculate the trapping of light emitted from a QD. Given the QD capability to isotropically absorb light over all angles of incidence, this study does not analyze the incident absorbed light, but instead, looks specifically at QD emission within the LSC.[6,12,20] We utilize Perfectly Matched Layer (PML) boundary conditions over a periodicity of 8 unit cells to accurately calculate behavior when the field emission has adequate distance to spatially decay while limiting coherent interference with the boundaries in each plane. In order to isolate emitters from coherent electric field phase interference, a supercell is required. Perfectly matched layer (PML) boundary conditions were used on all simulation boundaries in order to isolate the effects of coupling a single emitter to the PC optical environment. In order to approximate a QD, we use a dipole source. We simulate the source emission in the x, y, and z orientations then perform an average of the results weighted by the Purcell factor corresponding to each orientation. This averaging modeled the behavior of a single incoherent and nondirectional emitter. More than 20 positions for the rod array and more than 30 positions for the hole array were used to infer an ensemble average for a random dispersion of luminophores reported in Table 1.

The simulation consists of monitors surrounding the photonic crystal and the underlying substrate in order to record all light in every potential loss channel: the sides, the substrate, and the photonic crystal-to-air boundary. The monitors reported the percentage of emission that is lost to the ambient region above the photonic crystal, trapped in the plane of the photonic crystal, and propagated through the substrate. Monitors were placed in the substrate to record the fields that moved away from the photonic crystal and free space. These fields were then analytically propagated to the far-field to determine the power distribution incident on the flat, opposite surface of the substrate. The light that was trapped in plane and within these TIR angles of the substrate was considered trapped in the overall LSC system. Shape parameters such as the slab thickness, radius and so on, are all examined in normalized units, relative to the periodicity, as in ref 29.

The reflection, transmission, and absorption analysis of the photonic rod slab array demonstrated in Figure 6 was also done via Lumerical FDTD. Unlike the trapping analysis where the light source was a dipole emitter, the light source was a plane wave in order to simulate incoming light from the sun and the boundary conditions were periodic with an assumption of symmetry throughout the hexagonal rod array. Monitors were located both at the top and bottom of the array to account for reflected and transmitted light. Absorption was determined as the sum of reflection and absorption subtracted from 1.

MIT Photonic Bands (MPB) was used to calculate the photonic crystal band diagrams of Figure 7, using up to 32 k-points along each reciprocal space vector, with a resolution and mesh of 24 and 8, respectively.[49] The slab nature of the structure and the inherent periodicity of the method was reconciled by including a large portion of free space above/below the structure in the simulation volume such that confined fields did not interact.[50]

AUTHOR INFORMATION

Corresponding Author

Harry A. Atwater − *Department of Applied Physics and Materials Science, California Institute of Technology, Pasadena, California 91125, United States;* orcid.org/0000-0001-9435-0201; Email: haa@caltech.edu

Authors

Haley C. Bauser − *Department of Applied Physics and Materials Science, California Institute of Technology, Pasadena, California 91125, United States*

Colton R. Bukowsky − *Department of Applied Physics and Materials Science, California Institute of Technology, Pasadena, California 91125, United States; Leia Inc, Menlo Park, California 94025, United States*

Megan Phelan − *Department of Applied Physics and Materials Science, California Institute of Technology, Pasadena, California 91125, United States;* orcid.org/0000-0002-4968-7128

William Weigand − *School of Electrical, Computer, and Energy Engineering, Arizona State University, Tempe, Arizona 85287, United States*

David R. Needell − *Department of Applied Physics and Materials Science, California Institute of Technology, Pasadena, California 91125, United States*

https://dx.doi.org/10.1021/acsphotonics.0c00593
ACS Photonics XXXX, XXX, XXX−XXX

Zachary C. Holman − *School of Electrical, Computer, and Energy Engineering, Arizona State University, Tempe, Arizona 85287, United States*

Complete contact information is available at: https://pubs.acs.org/10.1021/acsphotonics.0c00593

Author Contributions

†H.C.B. and C.R.B. contributed equally to this work. The manuscript was written through contributions of all authors.

Notes

The authors declare no competing financial interest.

■ ACKNOWLEDGMENTS

This work was supported by the DOE "Photonics at Thermodynamic Limits" Energy Frontier Research Center under Grant DE-SC0019140 (D.R.N. and M.P.) and also by the by the Caltech Space Solar Power project (H.C.B.). Work by C.R.B., W.W., and Z.C.H. were supported in part by the Engineering Research Center Program of the National Science Foundation and the Office of Energy Efficiency and Renewable Energy of the Department of Energy under NSF Cooperative Agreement No. EEC-1041895.

■ REFERENCES

(1) Batchelder, J. S.; Zewai, A. H.; Cole, T. Luminescent Solar Concentrators. 1: Theory of Operation and Techniques for Performance Evaluation. *Appl. Opt.* **1979**, *18*, 3090−3110.

(2) Zhao, Y.; Lunt, R. R. Transparent Luminescent Solar Concentrators for Large-Area Solar Windows Enabled by Massive Stokes-Shift Nanocluster Phosphors. *Adv. Energy Mater.* **2013**, *3*, 1143−1148.

(3) Debije, M. G.; Verbunt, P. P. C. Thirty Years of Luminescent Solar Concentrator Research: Solar Energy for the Built Environment. *Adv. Energy Mater.* **2012**, *2*, 12−35.

(4) Sol, J. A. H. P.; Timmermans, G. H.; van Breugel, A. J.; Schenning, A. P. H. J.; Debije, M. G. Multi Luminescent Solar Concentrator "Smart" Windows. *Adv. Energy Mater.* **2018**, *8*, 1702922.

(5) Wu, K.; Li, H.; Klimov, V. I. Tandem luminescent solar concentrators based on engineered quantum dots. *Nat. Photonics* **2018**, *12*, 105−110.

(6) Needell, D. R.; et al. Design Criteria for Micro-Optical Tandem Luminescent Solar Concentrators. *IEEE Journal of Photovoltaics* **2018**, *8*, 1560−1567.

(7) Slooff, L. H.; Bende, E. E.; Burgers, A. R.; Budel, T.; Pravettoni, M.; Kenny, R. P.; Dunlop, E. D.; Büchtemann, A. A luminescent solar concentrator with 7.1% power conversion efficiency. phys. stat. sol. *Phys. Status Solidi RRL* **2008**, *2*, 257−259.

(8) Horowitz, K. A. W.; Remo, T.; Smith, B.; Ptak, A. Techno-Economic Analysis and Cost Reduction Roadmap for III-V Solar Cells. *Report NREL/TP-6A20-72103*; National Renewable Energy Laboratory, Golden, CO, 2018.

(9) Yablonovich, E. Thermodynamics of the fluorescent planar concentrator. *J. Opt. Soc. Am.* **1980**, *70* (11), 1362−1363.

(10) Smestad, G.; Ries, H.; Winston, R.; Yablonovitch, E. The thermodynamic limits of light concentrators. *Sol. Energy Mater.* **1990**, *21*, 99−11.

(11) Meinardi, F.; Ehrenberg, S.; Dhamo, L.; Carulli, F.; Mauri, M.; Bruni, F.; Simonutti, R.; Kortshagen, U.; Brovelli, S. Highly Efficient Luminescent Solar Concentrators based on Ultra-Earth-Abundant Indirect Band Gap Silicon Quantum Dots. *Nat. Photonics* **2017**, *11* (3), 177−185.

(12) Bronstein, N. D.; Yao, Y.; Xu, L.; O'Brien, E.; Powers, A. S.; Ferry, V. E.; Alivisatos, A. P.; Nuzzo, R. G. Quantum Dot Luminescent Concentrator Cavity Exhibiting 30-fold Concentration. *ACS Photonics* **2015**, *2* (11), 1576−1583.

(13) McDowall, S.; Butler, T.; Bain, E.; Scharnhorst, K.; Patrick, D. Comprehensive analysis of escape-cone losses from luminescent waveguides. *Appl. Opt.* **2013**, *52*, 1230−1239.

(14) Verbunt, P. P. C.; Sánchez-Somolinos, C.; Broer, D. J.; Debije, M. J. Anisotropic light emissions in luminescent solar concentrators−isotropic systems. *Opt. Express* **2013**, *21*, 485−493.

(15) van Sark, W.; Barnham, K. W. J.; Slooff, L. H.; Chatten, A. J.; Buchtemann, A.; Meyer, A.; McCormack, S. J.; Koole, R.; Farrell, D. J.; Bose, R.; Bende, E. E.; Burgers, A. R.; Budel, T.; Quilitz, J.; Kennedy, M.; Meyer, T.; Donega, C. D. M.; Meijerink, A.; Vanmaekelbergh, D. Luminescent Solar Concentrators: A review of recent results. *Opt. Express* **2008**, *16* (26), 21773−21792.

(16) Debije, M. G.; Van, M.-P.; Verbunt, P. P. C.; Kastelijn, M. J.; van der Blom, R. H. L.; Broer, D. J.; Bastiaansen, C. W. M. Effect on the output of a luminescent solar concentrator on application of organic wavelength-selective mirrors. *Appl. Opt.* **2010**, *49* (4), 745−51.

(17) Verbunt, P. P. C.; Tsoi, S.; Debije, M. G.; Boer, D. J.; Bastiaansen, C. W. M.; Lin, C.; de Boer, D. K. G. Increased efficiency of luminescent solar concentrators after application of organic wavelength selective mirrors. *Opt. Express* **2012**, *20*, 655−668.

(18) Leem, J. W.; Guan, X.-Y.; Yu, J. S. Tunable distributed Bragg reflectors with wide-angle and broadband high-reflectivity using nanoporous/dense titanium dioxide film stacks for visible wavelength applications. *Opt. Express* **2014**, *22*, 18519−18526.

(19) Baumeister, P. *Optical Coating Technology*; SPIE Press: Bellingham, Washington, U.S.A., 2004.

(20) Hanifi, D. A.; Bronstein, N. D.; Koscher, B. A.; Nett, Z.; Swabeck, J. K.; Takano, K.; Schwartzberg, A. M.; Maserati, L.; Vandewal, K.; van de Burgt, Y.; Salleo, A.; Alivisatos, A. P. Redefining Near-Unity Luminescence in Quantum Dots with Photothermal Threshold Quantum Yield. *Science* **2019**, *363*, 1199−1202.

(21) Yablonovitch, E. Inhibited spontaneous emission in solid-state physics and electronics. *Phys. Rev. Lett.* **1987**, *8* (20), 2059−2062.

(22) Liu, J.; Xu, H.; Yang, Z.; et al. A Research of Magnetic Control Ferrite Photonic Crystal Filter. *Plasmonics* **2017**, *12*, 971−976.

(23) Dudley, J.; Taylor, J. Ten years of nonlinear optics in photonic crystal fibre. *Nat. Photonics* **2009**, *3*, 85−90.

(24) Akahane, Y.; Asano, T.; Song, B.; et al. High-Q photonic nanocavity in a two-dimensional photonic crystal. *Nature* **2003**, *425*, 944−947.

(25) Andalib, P.; Granpayeh, N. All-optical ultracompact photonic crystal AND gate based on nonlinear ring resonators. *J. Opt. Soc. Am. B* **2009**, *26*, 10−16.

(26) Kurosaka, Y.; Iwahashi, S.; Liang, Y.; et al. On-chip beam-steering photonic-crystal lasers. *Nat. Photonics* **2010**, *4*, 447−450.

(27) Rousseau, I.; Wood, V. Nanophotonic luminescent solar concentrators. *Appl. Phys. Lett.* **2013**, *103*, 131113.

(28) Peters, M.; Goldschmidt, J. C.; Lö per, P.; Blasi, B.; Gombert, A. The effect of photonic structures on the light guiding efficiency of fluorescent concentrators. *J. Appl. Phys.* **2009**, *105*, No. 014909.

(29) Joannopoulos, J. D.; Johnson, S. G.; Winn, J. N.; Meade, R. D. *Photonic Crystals: Molding the Flow of Light*, 2nd ed.; Princeton University Press: Princeton, NJ, 2008.

(30) Ding, Y.; Magnusson, R. Band Gaps and Leaky-Wave Effects in Resonant Photonic-Crystal Waveguides. *Opt. Express* **2007**, *15*, 680−694.

(31) Purcell, E. *Phys. Rev.* **1946**, *69* (11−12), 674.

(32) Novotny, L.; Hecht, B. *Principles of Nano-Optics*, Cambridge University Press, 2006.

(33) Kuttge, M.; Garcia de Abajo, F.; Polman, A. Ultrasmall Mode Volume Plasmonic Nanodisk Resonators. *Nano Lett.* **2010**, *10* (5), 1537−1541.

(34) Jiao, X.; Blair, S. Optical Antenna Design for Fluorescence Enhancement in the Ultraviolet. *Opt. Express* **2012**, *20*, 29909−29922.

(35) Kristensen, P. T.; Hughes, S. Modes and Mode Volumes of Leaky Optical Cavities and Plasmonic Nanoresonators. *ACS Photonics* **2014**, *1* (1), 2−10.

https://dx.doi.org/10.1021/acsphotonics.0c00593
ACS Photonics XXXX, XXX, XXX−XXX

(36) Englund, D.; Fattal, D.; Waks, E.; Solomon, G.; Zhang, B.; Nakaoka, T.; Arakawa, Y.; Yamamoto, Y.; Vuckovic, J. Controlling the Spontaneous Emission Rate of Single Quantum Dots in a Two-Dimensional Photonic Crystal. *Phys. Rev. Lett.* **2005**, *95*, No. 013904.
(37) Lodahl, P.; Floris van Driel, A.; Nikolaev, I.; et al. Controlling the dynamics of spontaneous emission from quantum dots by photonic crystals. *Nature* **2004**, *430*, 654−657.
(38) Einstein, A. Strahlungs-Emission und -Absorption nach der Quantentheorie. *Verhandlungen der Deutschen Physikalischen Gesellschaft* **1916**, *18* (13/14), 318−323.
(39) Bukowsky, C. R. Scalable Nanophotonic Light Management Design for Solar Cells. *Thesis*, California Institute of Technology, 2019.
(40) Zhou, Y.; Benetti, D.; Fan, Z.; Zhao, H.; Ma, D.; Govorov, A. O.; Vomiero, A.; Rosei, F. Near Infrared, Highly Efficient Luminescent Solar Concentrators. *Adv. Energy Mater.* **2016**, *6*, 1501913.
(41) Meinardi, F.; Bruni, F.; Brovelli, S. Luminescent solar concentrators for building-integrated photovoltaics. *Nat. Rev. Mater.* **2017**, *2*, 17072.
(42) Needell, D. R.; Bukowsky, C. R.; Darbe, S.; Bauser, H.; Ilic, O.; Atwater, H. A. Spectrally Matched Quantum Dot Photoluminescence in GaAs-Si Tandem Luminescent Solar Concentrators. *IEEE J. Photovoltaics* **2019**, *9* (2), 397−401.
(43) Boccard, M.; Holman, Z. C. Amorphous silicon carbide passivating layers for crystalline-silicon-based heterojunction solar cells. *J. Appl. Phys.* **2015**, *118* (6), No. 065704.
(44) Bae, W. K.; Park, Y. S.; Lim, J.; Lee, D.; Padilha, L. A.; McDaniel, H.; Robel, I.; Lee, C.; Pietryga, J. M.; Klimov, V. I. Controlling the Influence of Auger Recombination on the Performance of Quantum-Dot Light-Emitting Diodes. *Nat. Commun.* **2013**, *4*, 2661.
(45) Likovich, E. M.; Jaramillo, R.; Russell, K. J.; Ramanathan, S.; Narayanamurti, V. High-Current-Density Monolayer CdSe/ZnS Quantum Dot Light-Emitting Devices with Oxide Electrodes. *Adv. Mater.* **2011**, *23*, 4521−4525.
(46) Caruge, J.; Halpert, J.; Wood, V.; et al. Colloidal quantum-dot light-emitting diodes with metal-oxide charge transport layers. *Nat. Photonics* **2008**, *2*, 247−250.
(47) Klimov, V. I.; Baker, T. A.; Lim, J.; Velizhanin, K. A.; McDaniel, H. Quality Factor of Luminescent Solar Concentrators and Practical Concentration Limits Attainable with Semiconductor Quantum Dots. *ACS Photonics* **2016**, *3* (6), 1138−1148.
(48) Meinardi, F.; Colombo, A.; Velizhanin, K.; et al. Large-area luminescent solar concentrators based on 'Stokes-shift-engineered' nanocrystals in a mass-polymerized PMMA matrix. *Nat. Photonics* **2014**, *8*, 392−399.
(49) Johnson, S. G.; Joannopoulos, J. D. Block-iterative frequency-domain methods for Maxwell's equations in a planewave basis. *Opt. Express* **2001**, *8* (3), 173−190.
(50) Johnson, S. G.; Fan, S.; Villeneuve, P.; Joannopoulos, J. D.; Kolodziejski, L. Guided Modes in Photonic Crystal Slabs. *Phys. Rev. B: Condens. Matter Mater. Phys.* **1999**, *60* (8), 5751−58.

https://dx.doi.org/10.1021/acsphotonics.0c00593
ACS Photonics XXXX, XXX, XXX−XXX